Electronics, Communications and Networks
A.J. Tallón-Ballesteros (Ed.)

doi:10.3233/FAIA241329

Optimized Non-Maximum Suppression for Multi-Source Local Discharge PRPD Pattern Identification

Yizhi FANG[a1], Yuling LIN[a], Tianshu LI[a], Zicong QIU[a], Yuhua HUANG[a], Xiabo YI [b]
[a] *Zhuhai Power Supply Bureau, Guangdong Power Grid Corporation, Zhuhai, Guangdong Province, China 519000*
[b] *Zhuhai Yite High tech Co., Ltd, Guangdong Zhuhai 519000, China*

Abstract. The multi-source partial discharge PRPD pattern can realize the pattern recognition of multi-source partial discharge types through the target detection algorithm training and identification of shape features. However, when the characteristics of different discharge pattern overlap, the small target is easily blocked by the large target, resulting in false detection and missed detection. Therefore, this paper proposes a multi-source partial discharge PRPD pattern identification algorithm with optimized non-maximum suppression. The Soft-NMS algorithm was introduced to solve the missed detection caused by overlapping targets; GIoU was used to replace the traditional IoU to calculate the similarity between targets and the loss function was optimized; the YOLOv7 network model was further built to identify the PRPD pattern of four typical discharges shape features. After cross-validation between simulation experiments and charged field data, the results prove that the average detection accuracy of the algorithm can reach 98.2% in simulation experiments and 88.4% in field experiments, effectively reducing the false detection rate and successfully identifying the characteristics of multi-source local discharge PRPD pattern when the targets overlap.

Keywords: Multi-source partial discharge; Target detection; PRPD Pattern; Soft-NMS; YOLOv7

1. Introduction

Gas Insulated Switchgear (GIS) is an indispensable component of the power system, renowned for its high voltage resistance, stability, and compact size [1]. Its introduction has supplanted numerous conventional and aging substations [2]. In most conventional substations, the majority of conductors are exposed, directly connecting electrical equipment [3]. This exposed connection method entails significant potential safety risks. In contrast to traditional substations, GIS offers advantages such as small footprint, extended maintenance cycles, minimal environmental interference, and exceptional stability, which are not inherent in traditional substations [4].

[1] Corresponding author: zhfyz@126.com

However, despite the significant advantages of GIS mentioned above, long-term practical operation has revealed that there are still deficiencies and potential hazards associated with GIS in substations due to various factors such as dust, metallic particles, corona discharge, gas voids, and bubbles [5]. These issues are difficult to avoid during the manufacturing, processing, transportation, and installation of GIS equipment. In the complex environment of high temperature and high pressure in the power system, various forms of partial discharge (PD) will occur in high-voltage equipment during long-term operation [6]. According to statistics from the China Electric Power Research Institute, the proportion of power system accidents caused by partial discharge increased annually, reaching 17.6%, 35.7%, and 45.0% from 2021 to 2023, respectively. Therefore, early detection of partial discharge occurrences and the identification of partial discharge types based on the characteristics of partial discharge signals associated with different insulation defects can guide the troubleshooting and operation management of GIS equipment [7].

The pattern recognition of partial discharge types has always been a fundamental issue in GIS Partial Discharge diagnosis, as identifying the type of PD occurring assists maintenance personnel in making timely targeted interventions [8]. Traditional pattern recognition algorithms typically involve manual feature extraction and classification, which heavily rely on human expertise, are subject to strong subjectivity, and exhibit low efficiency [9]. Currently, research in this field mainly focuses on single-source PD pattern recognition, essentially relying on the application of image classification algorithms [10]. However, image classification algorithms are unable to classify a single Phase-Resolved Partial Discharge (PRPD) pattern into multiple PD types [11]. Reference first proposed using object detection algorithms instead of image classification algorithms for training and recognition of PRPD pattern, achieving multi-source PD recognition at the PRPD pattern level [12]. However, when partial overlap occurs among the PD features in the pattern, it poses significant challenges to object detection, leading to cases of missed detections [13-15].

Therefore, to address the recognition challenges posed by overlapping targets (i.e., overlapping features in the PD pattern) in the current field of multi-source PD recognition, this paper proposes an optimized multiple-source PD PRPD pattern recognition algorithm by integrating the advantages of Soft Non-Maximum Suppression (Soft-NMS) algorithm with progressive suppression [16]. The Soft-NMS algorithm is introduced to resolve missed detection caused by overlapping targets [17]. Moreover, Generalized Intersection over Union (GIoU) is employed to replace traditional evaluation metrics for calculating the similarity between targets, optimizing the loss function. Furthermore, a You Only Look Once version 7 (YOLOv7) network model is constructed to identify the shape features of PRPD pattern for four typical discharges, reducing the missed detection rate when PD features overlap in the pattern and improving the reliability of multi-source PD pattern recognition.

2. Object Detection Algorithm

YOLO is a deep learning-based object detection algorithm, and its core idea is to treat the entire image as input and predict the classes and bounding boxes of multiple objects simultaneously using a single neural network [18]. As an end-to-end algorithm, it can be directly trained from raw PRPD pattern, avoiding the cumbersome manual feature

extraction process typically associated with traditional pattern recognition methods. This simplifies the implementation and training process of the algorithm [19].

Different from the partial discharge pattern recognition based on image classification algorithms, the object detection algorithm defines the partial discharge pattern features in the PRPD pattern as detection targets. It detects each partial discharge feature in the pattern and generates prediction boxes at the corresponding locations [20]. Since the YOLO algorithm can simultaneously predict the categories and positions of multiple objects, it can detect various types of partial discharge features simultaneously, thereby achieving the goal of detecting different partial discharge features in multi-source PRPD pattern. The specific algorithm principle is as follows:

The YOLO algorithm first divides the input PRPD pattern into S×S grids. For each grid, it predicts B bounding boxes and the probabilities of the classes of objects contained within these bounding boxes. Each bounding box is represented by five parameters: the center coordinates (x, y), the width (w), the height (h), and the confidence score indicating the presence of an object. Finally, NMS algorithm is applied to eliminate duplicate bounding boxes in the prediction results, yielding the final object detection results.

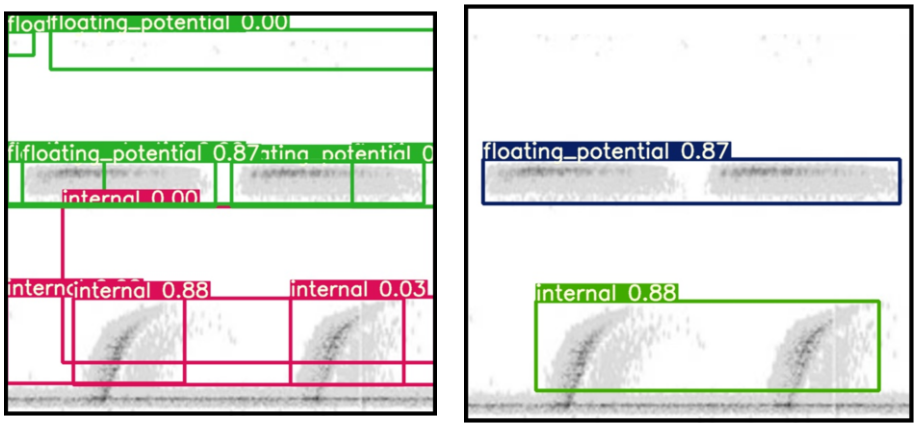

(a) (b)

Fig.1 Non-maximum Suppression

In Figure 1, a multi-source PRPD pattern, which has undergone grayscale processing and removed coordinate axes and grids, is depicted. Figure 1(a) illustrates the preliminary prediction boxes generated after algorithmic initial detection. Subsequently, based on the confidence score of each prediction box, redundant prediction boxes are eliminated using the NMS algorithm to obtain the final prediction results. However, in cases of target overlap, where two targets' prediction box positions are too close, the NMS algorithm may mistakenly classify the prediction box of the other target as redundant and remove it, resulting in missed detections.

3. The PRPD Pattern Recognition Algorithm based on Soft-NMS

This paper presents an optimized algorithm for multi-source partial discharge PRPD pattern recognition. It employs the YOLOv7 object detection algorithm for training and

recognizing multi-source partial discharge features. The workflow of the algorithm is depicted in Figure 2. The algorithm workflow includes:

1.Establishing an experimental platform, designing four types of partial discharge defects, training the model using single-source partial discharge PRPD pattern, and testing the algorithm using multi-source PRPD pattern.

2.Preprocessing the data, including grayscale conversion, normalization, and dimensionality reduction.

3.Employing the YOLOv7 algorithm for object detection, replacing traditional image classification algorithms.

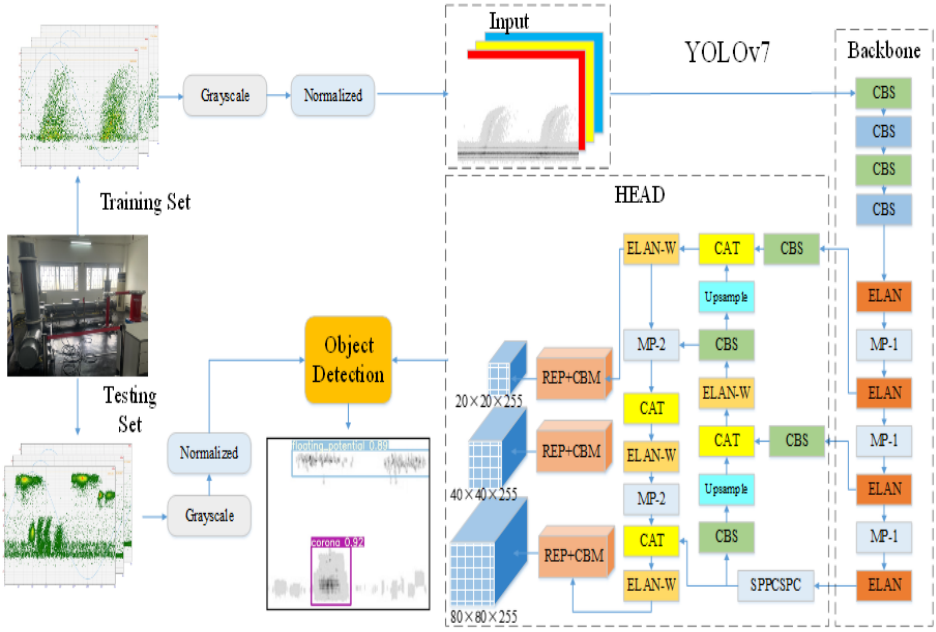

Fig.2 Algorithm Process

3.1. YOLOv7

Target detection is a critical task in recognizing pattern features in multi-source partial discharge PRPD pattern [21]. YOLOv7 is an efficient target detection algorithm, known for its improved accuracy and speed. In this paper, we focus on analyzing the advantages of YOLOv7 when dealing with overlapping targets.

YOLOv7 introduces Anchor-Scaled YOLOv7, where "Anchor" refers to predicted boxes. These boxes cover potential positions and sizes of pattern features. YOLOv7 treats each predicted box as an anchor, predicting the positions and sizes of partial discharge features [22]. The network structure the algorithm is depicted in Figure 3 Its network structure includes Input, Backbone, Neck, and Head networks. The Input section involves Mosic data augmentation and adaptive anchor box computation. Mosic randomly selects and processes multiple PRPD pattern to enrich the dataset and im-

prove robustness. During training, predicted boxes are generated based on initial anchor boxes and compared with ground-truth boxes to calculate the loss function.

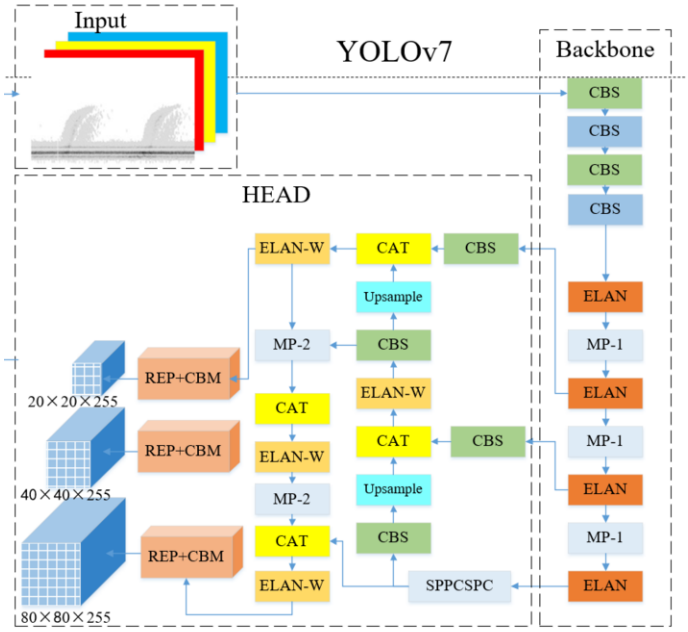

Fig.3 YOLOv7 network structure

The Backbone network is responsible for extracting image features, the Neck network merges these features, and the Head network predicts the position, size, and class information of target objects. YOLOv7 also introduces a technique called Spatial Pyramid Pooling (SPP) for feature extraction at different scales, as shown in Figure 4. SPP is a spatial pyramid pooling structure that uses max-pooling with kernels k={13×13, 9×9, 5×5, 1×1}, followed by concatenation of multi-scale feature maps. This effectively increases the receptive field of the backbone features, separating spatial features. These features, after multiple convolutions and pooling, are fed into the Head network for object detection. Additionally, YOLOv7 introduces techniques such as weakly supervised learning, label smoothing, and MixUp to further enhance the accuracy and robustness of the model.

When multiple overlapping feature maps are present, traditional object detection algorithms often encounter issues such as false positives or missed detections. However, YOLOv7 offers several advantages for better handling overlapping targets:

Firstly, YOLOv7 employs the Anchor-Scaled YOLOv7 algorithm, utilizing multiple prior boxes of different sizes and aspect ratios for detecting targets. This allows the algorithm to be more sensitive to variations in target sizes, thus better adapting to overlapping targets.

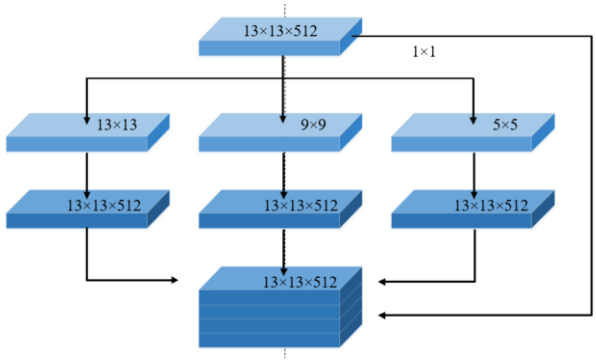

Fig.4 SPP network structure

Secondly, the Head network in YOLOv7 incorporates a branch structure designed to handle targets of different sizes. This branch structure can dynamically adjust detection accuracy and speed, thereby improving the handling of overlapping targets.

To accurately determine the confidence of detection boxes, this paper introduces an IoU prediction mechanism in YOLOv7. This mechanism predicts the IoU value for each detection box during object detection. During model training, YOLOv7 utilizes CIoU-loss to optimize the model, a loss function that better handles overlapping targets, further enhancing the model's accuracy.

3.2. Soft-NMS Algorithm

In object detection algorithms, when multiple detection boxes predict the same object, overlapping targets occur. Traditional (NMS) algorithms typically employ hard suppression to address overlapping targets. This involves comparing the overlaps of detection boxes to select the best one and suppressing redundant boxes. The principle is illustrated in Equation 1, where boxes with an IoU greater than a threshold have their scores set to 0. IoU represents the intersection over union ratio between different bounding boxes. However, when overlapping targets are severe, hard suppression methods have drawbacks such as being prone to missing detections and inaccurate suppression. This is because they only consider the confidence and overlap of individual detection boxes, disregarding correlations between multiple detection boxes.

$$S_i = \begin{cases} S_i, IoU(M, b_i) < N \\ 0, IoU(M, b_i) \geq N \end{cases} \tag{1}$$

In the equation, Si represents the score of the i-th predicted box; M represents the box with the highest score; bi represents the -th predicted box; N represents the set threshold.

3.3. GIoU Similarity

GIoU (Generalized Intersection over Union) is a widely used performance evaluation metric in object detection. It is based on a simple and intuitive principle that in the case of two overlapping shapes, the area of overlap should be the sum of the areas of the two shapes minus their intersection area. Therefore, the GIoU calculation formula

comprises three parts: IoU, GIoU, and an IoU compensation term, as shown in Equation 2:

$$GIoU = IoU - \frac{C - (A \bigcup B)}{C} \tag{2}$$

In the equation, C represents the bounding box that encloses both predicted box A and predicted box B.

Firstly, IoU stands for Intersection over Union, and it is used to measure the ratio of the intersection area of two shapes to their union area. Specifically, IoU is calculated as the intersection area of the two shapes divided by their union area, as shown in Equation 3:

$$IoU = \frac{A \bigcap B}{A \bigcup B} \tag{3}$$

In the equation, A and B represent two different predicted boxes.

Next, GIoU stands for Generalized Intersection over Union, which improves IoU by considering the distance between the bounding boxes of two shapes. GIoU is calculated as IoU minus the difference between the area of the minimum enclosing bounding box (the smallest rectangle that completely encloses both shapes) and their union area, divided by their union area.

Finally, the IoU compensation term refers to the compensation term in the GIoU formula, which is used to avoid unfairness when calculating overlapping targets. Traditional IoU measurements may lead to inaccuracies in cases of overlapping targets. Therefore, the IoU compensation term adjusts the IoU value to reduce errors between overlapping targets, mitigating penalties for predicting targets beyond the boundaries. This can improve the stability and accuracy of the model.

4. The Experimental Analysis

4.1. The Pre-processing

The pre-processing procedure for collected PD signals is as follows: initially, PD signals within a 10-second timeframe are acquired using a UHF data acquisition system. These signals are then subjected to a specific pattern generation program, resulting in the generation of a PRPD map with a resolution of 256×64. In this map, dark regions represent the occurrence frequency of signals, while light regions indicate background noise, as illustrated in Figure 5(a). Subsequently, the raw PRPD map undergoes denoising treatment. By identifying the maximum amplitude of pulses greater than 0 within each phase interval, a total of 64 values are obtained. The minimum value among these 64 values is designated as the baseline noise threshold. Any pulse amplitude below this threshold is then set to 0, effectively eliminating noise signals present at the bottom end. The denoising outcome is depicted in Figure 5(b). Following denoising, the PRPD map is subjected to phase resolution normalization, pulse count normalization, and amplitude normalization, as demonstrated in Figure 5(c). Finally, amplitude resampling is performed on the map. The amplitude axis, normalized post-resampling, is re-quantized according to a resolution of 64, resulting in the PRPD map shown in Figure 5(d), which is saved as a 64×64 two-dimensional array.

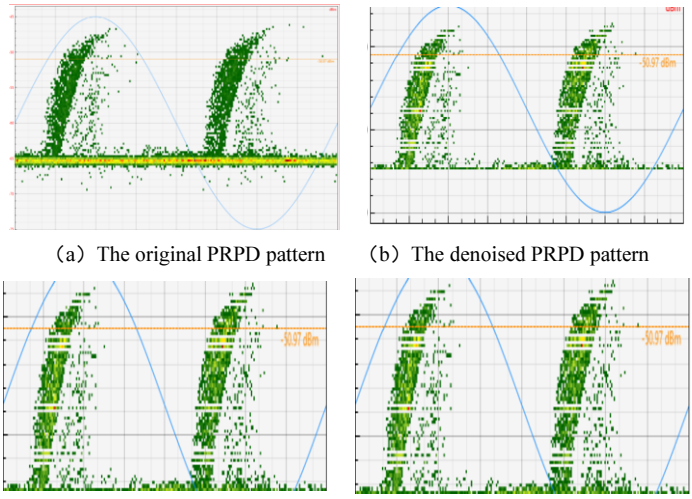

（a）The original PRPD pattern （b）The denoised PRPD pattern

（c）The normalized PRPD （d）The resampled PRPD

Fig.5 Signal pre-processing

Due to the color requirements of target detection algorithms for datasets (e.g., if the training set uses green pattern images, it can only recognize green pattern images), and because pattern saved by different manufacturers may have different colors, directly using pattern from one manufacturer as the training set would result in a model that cannot recognize pattern from other manufacturers, limiting its applicability. To enhance the algorithm's generalization and practical utility in engineering applications, we opted to standardize the pattern by converting them to grayscale. The grayscale representations of four typical partial discharge PRPD pattern are shown in Figure 6.

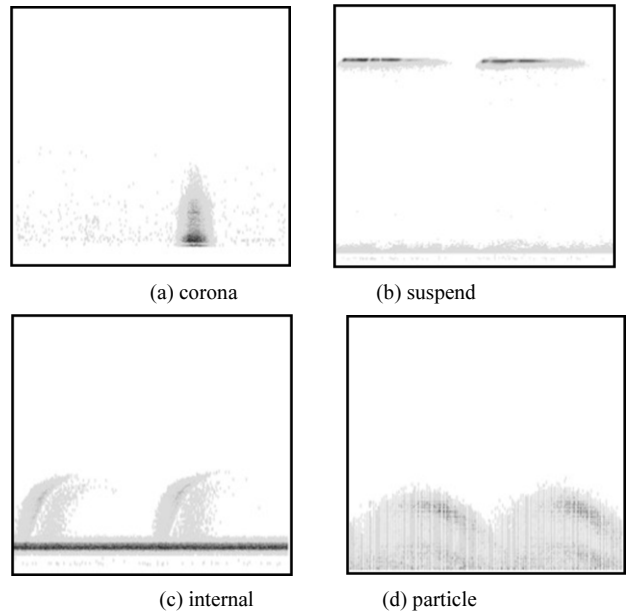

(a) corona (b) suspend

(c) internal (d) particle

Fig.6 Grayscale results

4.2. Simulation Experiment Analysis

The PRPD pattern collected from experiments include a total of 756 images, with 154 images of corona discharge + floating discharge, 126 images of corona discharge + internal discharge, 184 images of corona discharge + particle discharge, 137 images of floating discharge + internal discharge, and 155 images of floating discharge + particle discharge, as shown in Table 1. Due to variations in color and format preservation among different manufacturers for PRPD pattern, in order to mitigate the impact of color differences on model detection, both the training and testing sets were transformed into grayscale images, and the corresponding channel numbers within the model were adjusted accordingly.

Table 1 presents the distribution statistics of the dataset. A total of 1033 PRPD pattern from multiple sources of discharge were collected using the GIS simulation experimental platform. Among them, there were 154 images of corona discharge + floating discharge, 126 images of corona discharge + internal discharge, 184 images of corona discharge + particle discharge, 137 images of floating discharge + internal discharge, and 155 images of floating discharge + particle discharge. Through augmentation by Generative Adversarial Networks (GANs), the dataset was expanded to include 1540 images of corona discharge + floating discharge, 1260 images of corona discharge + internal discharge, 1840 images of corona discharge + particle discharge, 1370 images of floating discharge + internal discharge, and 1550 images of floating discharge + particle discharge.

Table 1 Data set distribution

	Discharge Types	Number of Samples Collecte	Number of Augmented Samples
Muti-source	corona+suspend	154	1540
	corona+internal	126	1260
	corona+particle	184	1840
	suspend+internal	137	1370
	suspend+particle	155	1550
	All	756	7560

The YOLOv7 network was trained using PyTorch on the specified hardware setup: GPU GeForce RTX 2060 Ti, CPU AMD Ryzen 7 4800H, running Windows 10 with CUDA 10.1 and OpenCV 4.5.5.

The training utilized a dataset split of 80% for training and 20% for validation. Training parameters included 300 epochs, with a learning rate of 0.01 for the first 100 epochs and 0.001 for the remaining 200 epochs. Each batch contained 16 sample images.

After training, the network successfully detected objects in the test set, displaying bounding boxes and labels for various patternl features, aligning with the experiment's objectives. The experimental results are shown in Figure 7. Successful identification of different types of partial discharge in multi-source PRPD pattern.

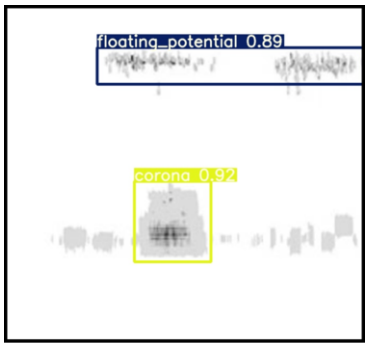

(a) corona+suspend

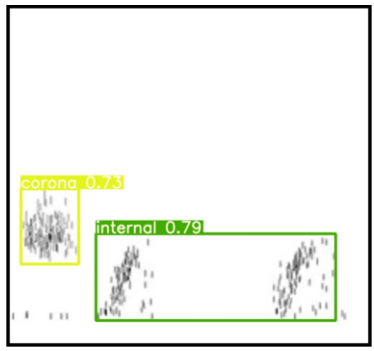

(b) corona+internal

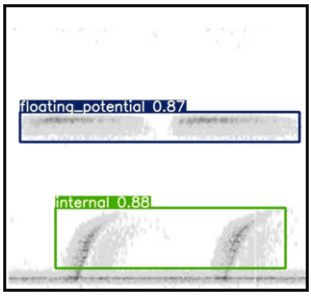

(c) internal+suspend

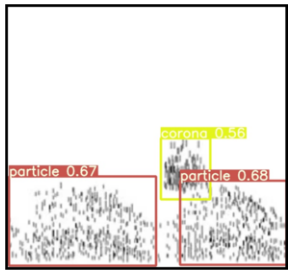

(d) corona+particle

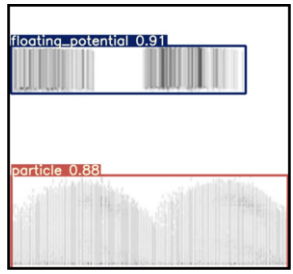

(e) suspend+particle

Fig.7 Detection effect

Define the following evaluation metrics: mean Average Precision (mAP), Precision, Recall, and Loss function. The specific formulas are as follows:

$$mAP = \frac{\sum_{i=1}^{N} AP_i}{N} \tag{4}$$

$$\mathrm{Re}\,call = \frac{N_{TP}}{N_{TP} + N_{FN}} \tag{5}$$

$$\mathrm{Pr}\,ecision = \frac{N_{TP}}{N_{TP} + N_{FP}} \tag{6}$$

Define the following evaluation metrics: mean Average Precision (mAP), Precision, Recall, and Loss function. The specific formulas are as follows:

Where:

NTP, NFP, and NFN represent the numbers of true positives, false positives, and false negatives respectively.

AP is the area under the Precision-Recall curve (P-R curve).

N is the number of detection categories.

Figure 8 compares the results of using the NMS algorithm and the Soft-NMS algorithm with the YOLOv7 network. As shown in the figure, before optimizing the NMS algorithm, the accuracy exhibited large fluctuations and poor convergence, oscillating around 93%; the recall gradually converged after 150 epochs, reaching 97%; the loss function steadily decreased, reaching 0.017 after completing 300 training epochs. After optimizing Soft-NMS, the accuracy significantly improved to 98%; the recall

also reached convergence after 150 epochs with a slight improvement; the loss function decreased to 0.013. In summary, all evaluation metrics of the proposed algorithm have been improved, and the convergence speed has been accelerated.

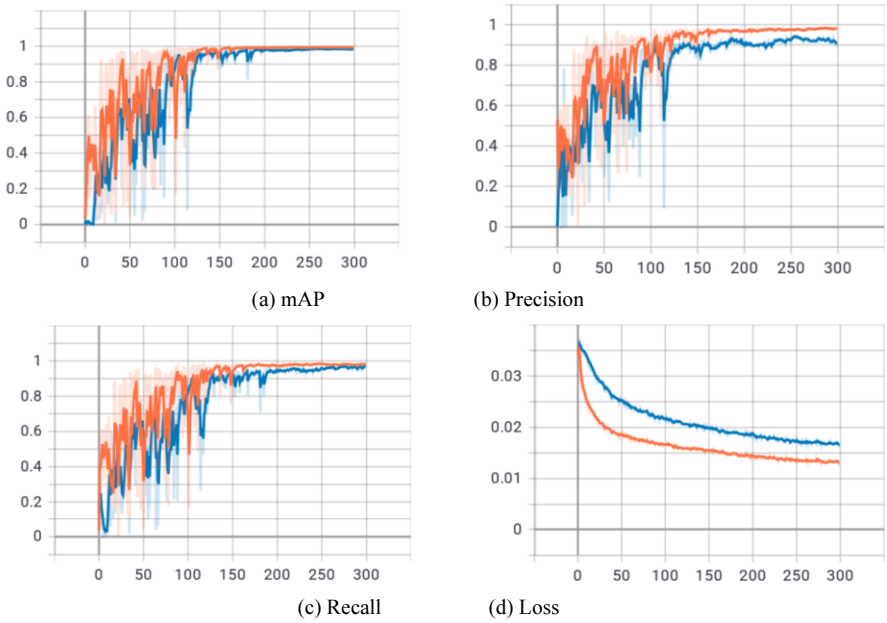

(a) mAP (b) Precision

(c) Recall (d) Loss

Fig.8 Before and after joining Soft-NMS

Table 2 Comparison of versions

Model	mAP
Yolo	0.82
Yolov2	0.85
SSD	0.952
YOLOv5	0.965
YOLOv7	0.964
The algorithm proposed in this paper	0.982

Table 2 presents the training and prediction results of various object detection algorithms on the dataset. Yolo and Yolov2, being relatively early algorithms, exhibit some shortcomings in detection accuracy, with mAP values of only 82% and 85%, respectively. The SSD model shows a significant improvement in detection accuracy, reaching up to 95.2%. YOLOv5 and YOLOv7 perform similarly, with the proposed algorithm in this paper achieving a mAP of 98.2%.

5. Conclusion

This paper proposes an optimized multi-source partial discharge PRPD pattern recognition algorithm by enhancing NMS using Soft-NMS algorithm to address missed

detections caused by overlapping targets. It utilizes GIoU to compute the similarity between targets, improving the loss function. Furthermore, a YOLOv7 network model is constructed to recognize the characteristic shapes of PRPD pattern for four typical discharge types, reducing missed detections caused by overlapping features and enhancing the reliability of multi-source partial discharge pattern recognition.

The effectiveness of the algorithm is validated using a pattern library collected from a 220kV field. It successfully detects multiple sources of partial discharge defects, achieving an average detection rate of 88.4%, demonstrating robustness.

Funding Project

Science and Technology Project 030400KK52220033 (GDKJXM20220875) funded by China Southern Power Grid Co., Ltd

References

[1] Zheng J, Chen Z, Wang Q, et al. GIS partial discharge pattern recognition based on time-frequency features and improved convolutional neural network[J]. Energies, 2022, 15(19): 7372.
[2] Liu T, Yan J, Wang Y, et al. GIS partial discharge pattern recognition based on a novel convolutional neural networks and long short-term memory[J]. Entropy, 2021, 23(6): 774.
[3] Zheng S, Wu S. Detection study on propagation characteristics of partial discharge optical signal in GIS[J]. IEEE Transactions on Instrumentation and Measurement, 2021, 70: 1-12.
[4] Tian J, Song H, Sheng G, et al. Knowledge-driven recognition methodology of partial discharge patterns in GIS[J]. IEEE Transactions on Power Delivery, 2021, 37(4): 3335-3344.
[5] Mahdi A S, Abdul-Malek Z, Arshad R N. SF 6 decomposed component analysis for partial discharge diagnosis in GIS: A review[J]. Ieee Access, 2022, 10: 27270-27288.
[6] Zaeni A, Halimi B, Khayam U. Design and Implementation of Experimental Setup for Measurement of Partial Discharge on GIS[C]//2021 3rd International Conference on High Voltage Engineering and Power Systems (ICHVEPS). IEEE, 2021: 132-136.
[7] Wang Y, Yan J, Ye X, et al. GIS partial discharge pattern recognition via a novel capsule deep graph convolutional network[J]. IET Generation, Transmission & Distribution, 2022, 16(14): 2903-2912.
[8] Yan J, Wang Y, Zhang W, et al. Domain-alignment multitask learning network for partial discharge condition assessment with digital twin in gas-insulated switchgear[J]. Measurement Science and Technology, 2024, 35(6): 065109.
[9] Yan J, Wang Y, Zhou Y, et al. A novel meta‐learning network for partial discharge source localization in gas‐insulated switchgear via digital twin[J]. IET Generation, Transmission & Distribution, 2024.
[10] Fang Y, Lin Y, Huang Y, et al. Automatic Localization of Partial Discharges in GIS Based on Digital Twins[M]//Electronics, Communications and Networks. IOS Press, 2024: 120-128.
[11] Qin Y, Arunan A, Yuen C. Digital twin for real-time Li-ion battery state of health estimation with partially discharged cycling data[J]. IEEE Transactions on Industrial Informatics, 2023.
[12] Chu X, Yu L, Tang B, et al. Partial Discharge Location in Transformer with Digital Twin Model[C]//Annual Conference of China Electrotechnical Society. Singapore: Springer Nature Singapore, 2023: 296-303.
[13] Wang Y, Yan J, Yang Z, et al. Deep domain-invariant long short-term memory network for partial discharge localization in gas-insulated switchgear[J]. IEEE Transactions on Power Delivery, 2023.
[14] F. C. Gu, “Identification of partial discharge defects in gas-insulated switchgears by using a deep learning method,” IEEE Access, vol. 8, pp. 163894–163902, 2020.
[15] M. Karimi, M. Majidi, H. MirSaeedi, M. M. Arefi, and M. Oskuoee, “A novel application of deep belief networks in learning partial discharge patterns for classifying corona, surface, and internal discharges,” IEEE Trans. Ind. Electron., vol. 67, no. 4, pp. 3277–3287, Apr. 2020.
[16] Liuhuo Wang, Kang Hou, and Lingqi Tan, “Research of GIS partial discharge type evaluation based on convolutional neural network,” AIP Advances 10, 085305 (2020).
[17] Moein Borghei and Mona Ghassemi, “A Deep Learning Approach for Discrimination of Single- and Multi-Source Corona Discharges,” IEEE Trans. Plasma Sci, vol. 49, no. 9, Sep. 2021.

[18] Redmon, J.; Divvala, S.; Girshick, R.; Farhadi, A. “You Only Look Once: Unified, Real-Time Object Detection,” IEEE 2016, 1, 779–788.
[19] Ruan, J. “Design and Implementation of Target Detection Algorithm Based on YOLO,” Beijing University of Posts and Telecommunications: Beijing, China, 2019.
[20] Redmon, J.; Farhadi, A. “YOLO9000: Better, Faster, Stronger. In Proceedings of the IEEE Conference on Computer Vision & Pattern Recognition,” IEEE, Honolulu, HI, USA, 21–26 July 2017; pp. 6517–6525.
[21] Q. Khan, S. S. Refaat, H. Abu-Rub and H. A. Toliyat, "Partial discharge detection and diagnosis in gas insulated switchgear: State of the art," IEEE Elect. Insul. Mag., vol. 35, no. 4, pp. 16-33, Jul. 2019.
[22] S. S. Udmale, S. K. Singh, R. Singh and A. K. Sangaiah, "Multi-Fault Bearing Classification Using Sensors and ConvNet-Based Transfer Learning Approach," IEEE Sensors J., vol. 20, no. 3, pp. 1433-1444, Feb. 1, 2020.